Korean J. Chem. Eng., 38(8), 1746-1755 (2021)
DOI: 10.1007/s11814-021-0809-1

pISSN: 0256-1115
eISSN: 1975-7220

Effect of glycidyl methacrylate-grafted poly(ethylene octene) on the compatibility in PLA/PBAT blends and films

Ye Zhang[*], Shiling Jia[*], Hongwei Pan[**], Lijuan Wang[*,†], Junjia Bian[,†], Yang Guan[***], Bohao Li[***], Huiliang Zhang[**,****], Huili Yang[**], and Lisong Dong[**]**

[*]School of chemical engineering, Changchun University of Technology, Changchun 130012, China
[**]Key Laboratory of Polymer Ecomaterials, Chinese Academy of Sciences, Changchun Institute of Applied Chemistry, Changchun 130022, China
[***]Jilin COFCO Biomaterial Co., Ltd., Changchun 130022, China
[****]Zhejiang Zhongke Applied Chemistry Technology Co., Ltd., Hangzhou 310000, China
(*Received 4 March 2021 • Revised 6 April 2021 • Accepted 11 April 2021*)

Abstract−A series of poly(lactic acid) (PLA), poly(butylene adipate-co-terephthalate) (PBAT) and glycidyl methacrylate-grafted poly(ethylene octene) (GPOE) blends and films with different GPOE content were prepared by melt blending and blowing film technique. The effect of GPOE on the rheological behavior, melt strength, crystallization behavior, crystallization morphology, miscibility, mechanical property, phase morphology, thermal stability and water vapor permeability were studied. The addition of GPOE improved melt rheological properties. Results of DSC showed that addition of GPOE encouraged the mobility of PLA molecular chains and enhanced crystalline ability. POM observations revealed that the addition of GPOE made the density of spherulite nucleation increase and the size of crystalline particles decrease. From DMA and SEM analysis, it was demonstrated that PLA/PBAT blend was an immiscible system and GPOE in the blend could improve compatibility between PLA and PBAT. Results of mechanical test showed that the PLA/PBAT/GPOE blends and films obtained had excellent mechanical properties. The elongation at break of 50/30/20 w/w/w PLA/PBAT/GPOE blend (477%) was higher by about 2.2 times than that of 70/30/0 w/w/w PLA/PBAT/GPOE blend (220%). The tensile strength of all the PLA/PBAT/GPOE blends exceeded 31 MPa. The tensile strength reached 32.9 MPa (MD) and 22.5 MPa (TD), the elongation at break exceeded 210% and tear strength exceeded 140 kN/m for 50/30/20 w/w/w PLA/PBAT/GPOE film. With increasing GPOE content, thermal stability and water vapor barrier property also improved.

Keywords: Poly(lactic acid), Poly(butylene adipate-co-terephthalate), Glycidyl Methacrylate-grafted Poly(Ethylene Octene), Compatibilizer, Films

INTRODUCTION

The development of social economy promotes the rapid development of the material packing field. Most packing materials are petrol-based polymers, such as polypropylene (PP), polyethylene terephthalate (PET), polyethylene (PE) and polystyrene (PS), which are not biodegradable. A significant amount of polymer packing materials are produced and used every day and with most of the biodegradable discarded after a single use. These non-biodegradable polymer packing materials usually end up either in a landfill or directly to the natural environment [1]. Hence, the large-scale production and consumption of petrol-based polymer packing materials have created several problems: waste of energy and resources, environmental pollution, and harm to animals and ecosystem caused by discarded plastics. Most of the bio-polymers are derived from renewable resources that can help to save fuels/energy. Moreover, their biodegradability can be exploited to save landfills [2]. Therefore, biodegradable biopolymers have attracted considerable research attention from academia and various industries due to environmental pollution and continuous reduction of petroleum resources.

Polylactide or poly(lactic acid) (PLA) is one of the most commercial biobased-biodegradable polymers, whose monomer, L-lactic acid, can be derived from biomass (corn, cassava or sugar beets) and can eventually be converted to carbon dioxide, water and humus [3,4]. In addition to high biodegradability and renewability, PLA also has high mechanical strength, optical transparency, high gloss and excellent processability [5-9]. Therefore, it is a promising and viable alternative to petroleum-based polymers that can be widely used in many fields, such as daily life containers, textiles, disposable tableware, packaging bags, other disposal products and biomedical devices as suture, tissue engineering, controlled release systems [10-12]. However, PLA also has inherent drawbacks in some properties including low impact strength less than 5 kJ/m^2, brittleness with elongation at break lower than 10%, low glass transition temperature around 60 °C, and poor thermal stability [13-15]. These major drawbacks severely limit its large-scale commercial application. Therefore, numerous strategies, including copolymerization, blending, compounding and additives, have been adopted to improve PLA's relevant properties [16]. Blending of PLA with other polymers is a practical and economical approach to fabricate blends with a favor-

[†]To whom correspondence should be addressed.
E-mail: wanglj15@ccut.edu.cn, bianjunjia@ciac.ac.cn

able performance combination of the components.

To improve impact strength of poly(lactic acid), Jin et al. [17] used SiO_2 nanoparticles whose surface was treated with oleic acid to prepare PLA/PBS/SiO_2 nanocomposites by solution blending. Their results indicated that improved impact strength of PLA was achieved without sacrificing the thermal and mechanical properties of the nanocomposites. Natthapong et al. [18] studied morphology, thermal and mechanical properties of PLA/PVA blends with a composition of 70/30, 60/40, and 50/50 wt%. Their results showed that an increase in the PVA content improved blend morphology by phase conversion from sea-island to co-continuous morphology. Zhang et al. [19] studied PLA/PHB blends at a number of different weight ratios. The results indicated that PLA/PHB blends are immiscible and a PLA matrix with a 25 wt% of PHB exhibits significantly improved tensile properties compared with pure PLA due to the reinforcement effect of the small finely dispersed PHB crystals. Many other polymers also could use to blend with PLA, such as poly(ε-caprolactone) (PCL) [20], poly(propylene carbonate) (PPC) [21], ethylene/n-butyl acrylate/glycidyl methacrylate (EBA-GMA) [22], poly(ethylene-co-vinyl alcohol) (EVOH) [23], polyurethane (TPU) [24]. Poly(butylene adipate-co-terephthalate) (PBAT) is a biodegradable aliphatic-aromatic copolyester and a commercial product with low elastic modulus and high elongation-to-break. In view of its biodegradability and performance, which are similar to that of a thermoplastic, PBAT is a promising candidate for toughening of PLA [25]. However, PBAT is immiscible with PLA according to some reports [26-28] and their immiscibility can result in unsatisfactory mechanical properties of the blends. Compatibilizer and reactive compatibilization are effective methods to improve miscibility or compatibility between PLA and PBAT [29,30].

Based on the above discussion, glycidyl methacrylate-grafted poly(ethylene octene) (GPOE) was used as the reactive compatibilizer to enhance the compatibility between PLA and PBAT with the aim of obtaining high performance materials because both PLA and PBAT contain reactive carboxylic acid and hydroxyl groups that can react with the high reactive epoxide groups of GPOE in the melt state. The obtained biodegradable blends and films were characterized using various analytical methods.

EXPERIMENTAL

1. Materials

Poly(lactic acid) pellets with 98% L-lactide content (Natureworks 4032D, M_W=207,000 g·mol^{-1}, M_W/M_n=1.59) were provided by American Natureworks Company. A commercially available poly(butylene adipate-co-terephtalate), PBAT, was supplied by Xinjiang Blue Ridge Tunhe Polyester Co., Ltd. Glycidyl methacrylate-grafted poly(ethylene octene) (grafted ratio 3 wt%) abbreviated as GPOE in this article were supplied by Amoy Coace Plastic Technology Co., Ltd., China.

2. Sample Preparation

PLA, PBAT and GPOE pellets were dried at 70 °C for 8 h in a vacuum oven, respectively. The blends were prepared using a co-rotating twin-screw extruder with nine heating zones (SHJ-20, Lanzhou Lantai Plastics Machinery Engineering Co. Ltd., Lanzhou, China, L/D=36). The mixing compositions of PLA, PBAT, and GPOE blends were 70/30/0 w/w/w, 65/30/5 w/w/w, 60/30/10 w/w/w, 55/30/15 w/w/w, and 50/30/20 w/w/w, respectively. The extrusion temperature ranged from 175 to 195 °C. Then, all the samples were compression molded into sheets with thickness of 1.0 mm at 190 °C under 10 MPa for rheological measurements test and mechanical properties test. The blend films were fabricated by blowing using a smooth-bore single-screw extruder with processing temperature at different zones in the range of 185 °C to 195 °C.

3. Characterization

3-1. Rheological Measurements

Melt rheological measurements were done by using a parallel plate rheometer (AR 2000ex, TA, USA). Samples with thickness of about 1 mm were placed between the plates with diameter of 25 mm and frequency sweep tests were done at 190 °C in a frequency range from 0.1 to 100 Hz.

3-2. Melt Strength (MS)

A capillary rheometer (Rosand RH-7, Britain) was used to investigate melt strength (MS) of PLA/PBAT/GPOE blends. Experiments were carried out at 185 °C. Samples of approximately 25 g were preheated in a cartridge for 3 min and then compacted, with the process repeated twice. It can be used to determine the uniaxial extensional performance of polymer melts.

3-3. Differential Scanning Calorimetry (DSC)

Thermal properties of PLA/PBAT/GPOE blends were studied with differential scanning calorimetry (TA Instruments DSC Q20 USA) under nitrogen atmosphere with a gas flow rate of 50 ml/min. The samples (about 5 to 8 mg) were first heated to 190 °C for 3 min to remove the heating history. Then, the samples were cooled to −60 °C and heated again to 190 °C. The heating and cooling rate was 10 °C/min. The thermal properties of the blends could be obtained from the heating scans. By measuring the heat of fusion (ΔH_f), the degree of crystallinity (X_c) was determined using the following equation:

$$X_c = \frac{\Delta H_f}{w_{PLA} \times \Delta H_f^0} \times 100\% \quad (1)$$

where ΔH_f is the heat of fusion, ΔH_f^0 is the heat of fusion for 100% crystalline PLA (93.6 J/g) [31] and w_{PLA} is the weight fraction of PLA.

3-4. Crystallization Morphology

Spherulitic morphologies of the blends were observed, using a DM4500P (Leica, Germany) POM equipped with a THMS 600 hot stage (Linkam, UK). The samples were first placed between two glass slides and then compressed. First, the samples were heated from room temperature to 190 °C at a rate of 10 °C/min, maintained for 3 min to eliminate thermal history. The samples were then cooled to 120 °C at the rate of 50 °C/min. Next, the samples were kept for 60 min in isothermal conditions. The final spherulite morphologies and size were recorded.

3-5. Wide-angle X-ray Diffraction (WAXD)

Wide-angle X-ray diffraction (WAXD) spectra were recorded on D8 ADVANCE BRUKER X-ray diffractometer (Karlsruhe, Germany) to characterize the crystalline structure of the blends. The Cu Kα radiation (k=1.54 Å) source was operated at a current of 40 mA and voltage of 50 kV. The scattering angle (2θ) ranged from 5° to 50° at a scanning speed of 3°/min. Before testing, the samples were melting at 190 °C for 10 min, then quenched at 120 °C for 1 h

to obtain complete crystal.

3-6. Dynamic Mechanical Analysis

Dynamic mechanical analysis of the blends was performed with a DMA instrument (DMA 850, TA Instrument, Co., USA) in the tensile mode. Tensile bar specimens (20×4×1 mm) were used for testing. The temperature ranged from −80 to 130 °C, with a heating rate of 3 °C min^{-1}. The oscillating frequency and amplitude of the test were 1 Hz and 20 μm, respectively. The preload was 0.01 N before the experiment.

3-7. Mechanical Properties

The tensile property of the samples was determined with an Instron 1211 testing machine according to ASTM D638-2008 standard. The samples of the PLA/PBAT/GPOE blend were punched out from the compression molded sheets. The dimension of dumbbell-shaped samples was 20×4×1 mm (L×W×H), where L, W, and H are the span length, width, and thickness, respectively. Prior to testing, all samples were pre-conditioned for 24 h at room temperature and 50% relative humidity controlled environment. The crosshead speed of all tests was kept at 20 mm/min. At least five runs for each sample were measured and the results were averaged.

The tensile property of the PLA/PBAT/GPOE films was also studied using an intelligent electronic tensile testing machine model XLW-100N (Labthink Languang Corp., China). Cutting strips (100×15×0.025 mm^3) for tensile tests were cut from the previously blown films in both machine direction (MD) and transverse direction (TD). A tensile test was conducted at room temperature according to GB/T 1040.1-2006 standard at a cross head speed of 200 mm/min. Five specimens of each PLA/PBAT/GPOE film sample were tested to get an average value.

The rectangular PLA/PBAT/GPOE film samples with a dimension of 100×13×0.2 mm were cut from the previously blown films in both machine direction (MD) and transverse direction (TD). The right angle tearing strength was determined using an intelligent electronic tensile testing machine model XLW-100N (Labthink Languang Corp., China) at about 25 °C according to QB/T 1130-91 (China) standard at a crosshead speed of 50 mm/min. The tear strength values were obtained based on the average tear results of at least five tear specimens.

3-8. Scanning Electron Microscopy (SEM)

In morphology analysis, a field emission scanning electron microscope (model Germany Merlin Zeiss) was used to observe the phase morphology of the PLA/PBAT/GPOE blends at an accelerating voltage of 1 kV. The extruded PLA/PBAT/GPOE blends were fractured in liquid nitrogen for 30 min and covered with gold to enhance the electron conductivity before examination with the SEM.

3-9. Thermogravimetric Analysis (TGA)

The thermal stability of the PLA/PBAT/GPOE films weighing about 10 mg was performed with a Netzsch TG209 analyzer at a heating rate of 10 °C/min from 30 to 600 °C in a nitrogen atmosphere to protect the samples from being oxidized. The weight loss of the blend films was determined from TGA curves. The degradation temperature at the maximum degradation rate (T_{max}) for each stage was determined from the first derivative of the TGA curves (DTG).

3-10. Water Vapor Transmission Rate (WVTR)

The water vapor transmission (WVTR) rate through the PLA/PBAT/GPOE films was determined using a water vapor transmission instrument (PERME W3/060) based on the ASTM standard, E96/E96 M-05. The PLA/PBAT/GPOE films were cut into 7.4 cm diameter circles and the thicknesses were measured. The films were placed in test dishes and the test temperature was 38 °C and relative humidity was 90%. An average value from three parallel measurements was reported as g·cm/cm^2·Pa·s.

RESULTS AND DISCUSSION

1. Melt Rheological Properties

The analysis of rheological properties is particularly helpful in research on polymer blends and the processability of the blends. Rheological properties of blends are related to their miscibility, morphology/phase structure and the interaction between the components. Dynamic rheological experiments were conducted for the PLA/PBAT/GPOE blends over the whole composition range. The storage modulus represents the elastic character of blends or the energy stored in the deformation. The storage modulus (G′) versus angular frequency obtained from dynamic rheological experiment is shown in Fig. 1. At low frequency, the G′ was several times higher than that of a blend without GPOE and increased monotonically with the GPOE content. However, the incorporation of GPOE had less effect on the G′ of melts at higher frequency. The improvement of the G′ values due to the addition of GPOE indicated the formation of entangled structures among PLA chains, PBAT chains and GPOE. An additional factor strengthening G′ for the PLA/PBAT/GPOE blends was the formation of PLA-co-PBAT copolymers at the PLA/PBAT interface due to epoxy groups of GPOE, which led to a reduction in the size of the dispersed phase and an increase of the active surface of interaction between the blend components. Similar results were observed by Jacek et al. [32], where the same type of a multifunctional modifier was used for PLA/PBAT blends.

Fig. 2 shows the relationship between loss modulus (G″) and angular frequency of the PLA/PBAT/GPOE blends. The loss modulus is related to the energy dissipated in the flow or the viscous character [33]. It indicated that G″ of all blends increased with

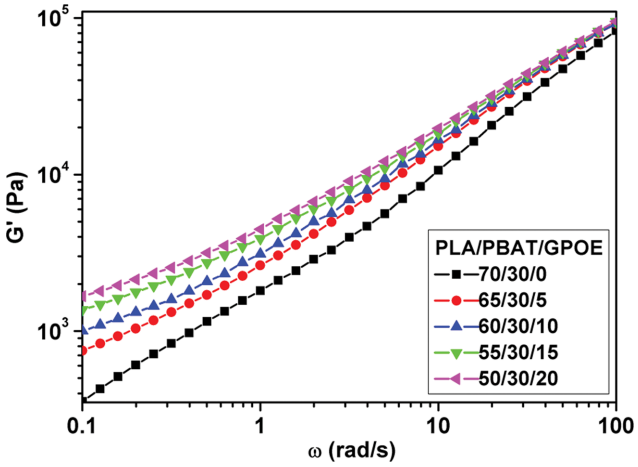

Fig. 1. Plots of storage modulus versus angular frequency for PLA/PBAT/GPOE blends.

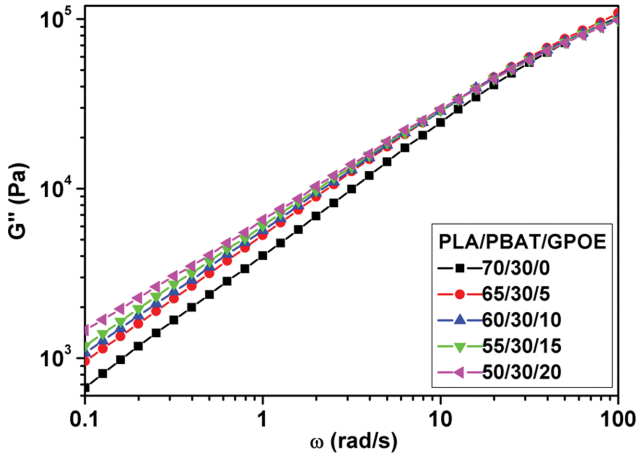

Fig. 2. Plots of loss modulus versus angular frequency for PLA/PBAT/GPOE blends.

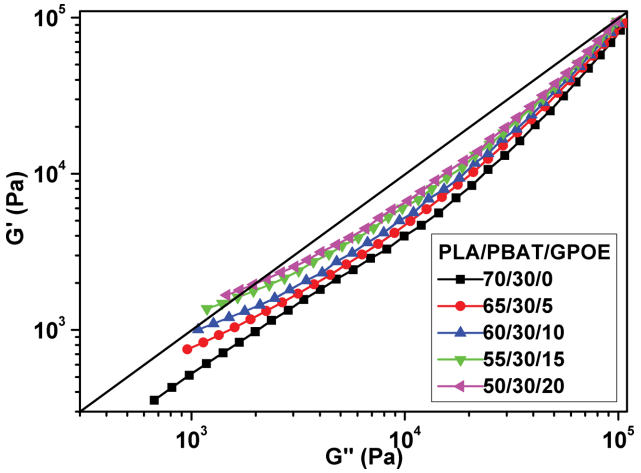

Fig. 4. Han plots of dynamic storage modulus (G′) versus dynamic loss modulus (G″) for the PLA/PBAT/GPOE blends.

angular frequency. At high frequency, the movement of polymer molecular chains in the blends increased, which led to an increase of loss energy in the blend. The increase in GPOE content improved interfacial adhesion and entanglement, thus G″ was improved. This result was similar to the situation of the storage modulus described above. The much higher loss modulus indicates higher viscosity. The melts in the presence of GPOE had higher G′ and G″, which indicated that the addition of GPOE truly changed the rheological properties of PLA/PBAT blends.

The complex viscosity (η^*) of the PLA/PBAT/GPOE blends is shown as Fig. 3. As we can see from Fig. 3, all samples displayed a shear-thinning tendency, which indicated a classical liquid-like behavior of the polymer melt [3]. When the content of GPOE increased, η^* of the PLA/PBAT/GPOE blends increased at nearly all frequencies. This result could be due to the reaction and entanglement structures increased among PLA, PBAT and GPOE with increasing GPOE content, which made mobility of polymer chains difficult. Thus, the η^* increased. The enhancement of η^* is beneficial in film extrusion.

In melting state, the Han plot (G′ versus G″) is an important characterization of the viscoelastic properties of polymer materials. Fig. 4 shows the Han plots for the PLA/PBAT/GPOE blends and the straight line (G′=G″) divides the coordinate into two parts and determines the transition. Below the straight line, the polymer materials present major viscosity behavior; conversely, they exhibit elasticity behavior [34]. As we can see from Fig. 4, Han plots of the PLA/PBAT/GPOE blends were almost located below the straight line of G′=G″, which proved that these blends with different amounts of GPOE were more viscous than elastic components at the melting state. As noted, the reduced slope with the addition of GPOE indicated that the blends became more heterogeneous. When GPOE loading was high, physical and chemical association within the blends increased; thus, much energy was needed to change the degree of heterogeneity [35]. In addition, the elastic behavior of the PLA/PBAT/GPOE blends was enhanced with increasing GPOE content, which was significant for blown films and practical production process.

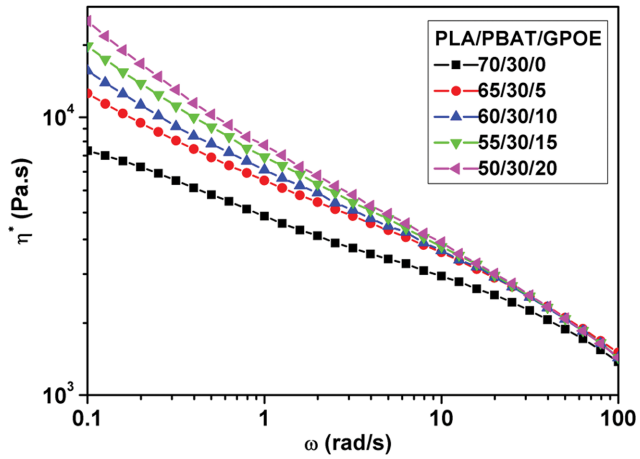

Fig. 3. Plots of complex viscosity versus angular frequency for PLA/PBAT/GPOE blends.

2. Melt Strength (MS)

Melt strength of the PLA/PBAT/GPOE blends is presented in Fig. 5. The addition of GPOE brought about an increase in MS of

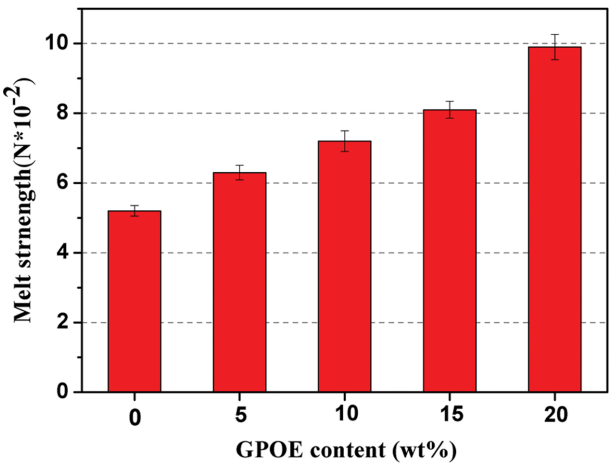

Fig. 5. The melt strength of the PLA/PBAT/GPOE blends.

blends. The melt strength increased from 0.052 N to 0.099 N with increasing GPOE content from 0 to 20 wt%. These results showed that crosslinking reaction among GPOE, PLA, and PBAT had taken place; thus intermolecular entanglement increased. The higher the entanglement there, the greater the melt strength will be. The enhancement of melt strength is beneficial for the processing technologies involving injection molding, blow molding, thermoforming, spinning.

3. Differential Scanning Calorimetry (DSC)

Fig. 6 displays the second heating DSC profiles of the PLA/PBAT/GPOE blends, and the corresponding thermal parameters are summarized in Table 1. In the thermogram, the glass transition temperature (T_g) of GPOE is not visible and it must occur around −40 °C according to related literature [36]. The T_g of PBAT in blend was about −28.7 °C and the T_g of PLA in blend without GPOE was observed at 60.3 °C. The T_g of PLA was observed to decrease slightly through the inclusion of increasing amount of GPOE. There were still two glass transitions relative to the PLA and PBAT phases for the PLA/PBAT/GPOE blend, which implies that the PLA/PBAT was still thermodynamically immiscible system despite the GPOE being added [37]. However, there was something different in the crystallization behavior of the blends with and without GPOE added. During heating PLA in the PLA/PBAT blends without GPOE had a cold crystallization peak, an exothermic signal at 100.1 °C. Compared with the PLA/PBAT blends without GPOE, the cold crystallization temperature (T_{cc}) and melting temperature (T_m) of the PLA/PBAT/GPOE blends decreased with the addition of GPOE. Moreover, the degree of crystallinity (X_c) of PLA in the blends increased. For example, the X_c of 70/30/0 w/w/w PLA/PBAT/GPOE blend sample was 38.0%, smaller than that of

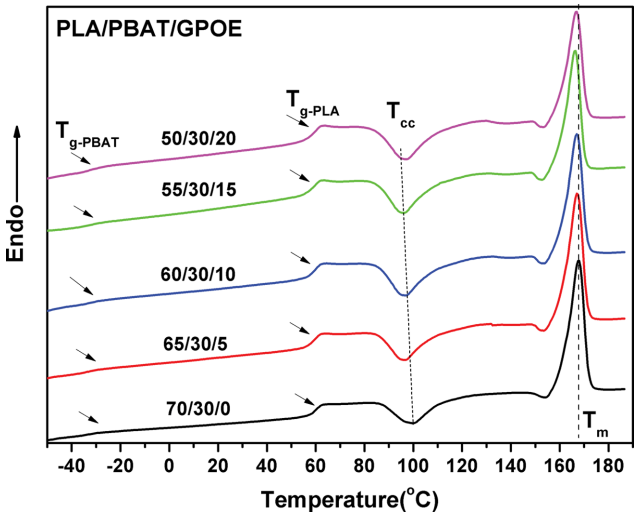

Fig. 6. DSC curves of the PLA/PBAT/GPOE blends in the second heating run.

Table 1. Thermal and crystalline properties of the PLA/PBAT/GPOE blends

PLA/PBAT/GPOE (W/W/W)	$T_{g\text{-}PLA}$ (°C)	T_{cc} (°C)	T_m (°C)	ΔH_{cc} (J/g)	ΔH_f (J/g)	X_c %
70/30/0	60.3	100.1	168.7	8.1	24.9	38.0
65/30/5	60.1	96.8	167.0	9.5	24.0	39.4
60/30/10	59.9	97.0	166.9	10.5	22.7	40.4
55/30/15	59.7	96.5	166.5	11.9	21.6	42.0
50/30/20	59.3	97.3	166.7	13.2	20.9	44.7

T_g: glass transition temperature; T_{cc}: cold crystallization temperature; ΔH_{cc}: cold crystallization enthalpy; T_m: melting temperature; ΔH_m: melting enthalpy; X_c: degree of crystallinity.

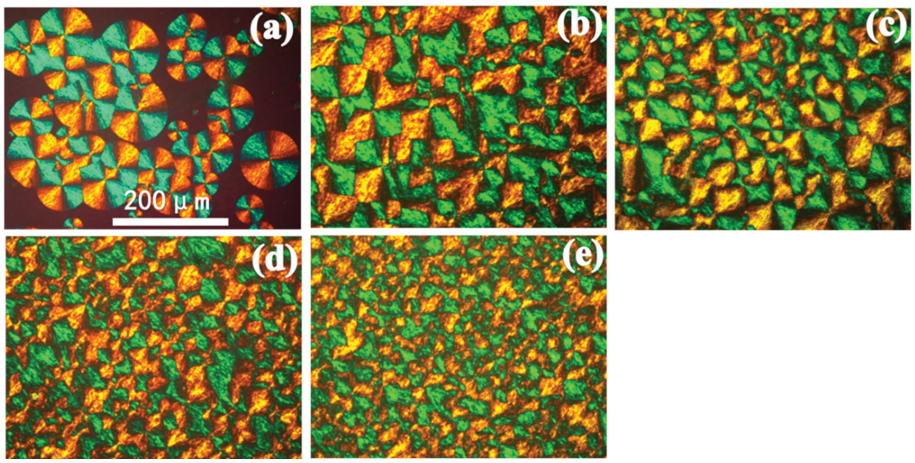

Fig. 7. POM images of isothermal crystallization at 120 °C for 60 min: (a) 70/30/0 w/w/w, (b) 65/30/5 w/w/w, (c) 60/30/10 w/w/w, (d) 55/30/15 w/w/w, and (e) 50/30/20 w/w/w for the PLA/PBAT/GPOE blends.

other samples, indicating that the addition of GPOE could encourage the mobility of PLA molecular chains [38], enhance crystalline ability and speed up the crystallization rate; as a consequence, the X_c of the PLA component in the blend slightly increased. Similar behavior was also reported by Aliotta et al. [39].

4. Crystallization Morphology of the PLA/PBAT/GPOE Blends

POM analysis was performed to analyze the effect of the incorporated GPOE on the spherulitic morphology of PLA in blends. Fig. 7 shows the POM micrographs of the PLA/PBAT/GPOE blends isothermally melt crystallized at 120 °C. The spherulitic morphology of 70/30/0 w/w/w PLA/PBAT/GPOE blend formed well-defined spherulites with a size of approximately 80 μm in diameter that exhibited the classical Maltese-cross extinction pattern, as shown in Fig. 7(a) [40,41]. With the addition of 5 wt% GPOE in blend, the density of spherulite nucleation increased spherulites and, as a result, the spherulite size became smaller, as observed from the Fig. 7(b). From Fig. 7(c) to Fig. 7(e) with the further increase the GPOE content, the nuclei density increased significantly and the size of the spherulites decreased obviously. The shrinking of the spherulite size may have arisen from the fact that more nuclei density made the spherulites prone to impinge on their neighbors to hinder further growth, resulting in smaller spherulites. As a result, spherulite morphology of the samples was rough and it was hard to identify the Maltese-cross extinction pattern. The reason for the increased nuclei density was that the branching points among molecular chains could act as heterogeneous nucleation sites for the crystallization of PLA [38,42] and the addition of GPOE increased the molecular chain mobility of PLA [38], which promoted the nucleation ability of PLA, that was in consistent with the DSC results. However, the content of GPOE in the blends did not show an obvious effect on the morphology of spherulites. Additionally, the addition of GPOE afforded smaller spherulites, which is beneficial for the improvement of toughness.

5. Wide Angle X-ray Diffraction (WAXD) Analyses

The X-ray diffraction is often used to analysis the structure variation of crystalline polymer. WAXD technique is utilized to investigate the crystalline structure and morphology. To get further information about the crystal structure of PLA/PBAT/ADR blends, wide-angle X-ray diffraction (WAXD) experiments were performed in this study. Fig. 8 shows representative WAXD curves of PLA/PBAT/GPOE blends with different GPOE content isothermally crystallizing for 1 h at 120 °C. In the XRD analysis, several characteristic diffraction peaks are seen, [0, 1, 0], [2, 0, 0/1, 1, 0], [2, 0, 3], and [0, 1, 5] at diffraction angles 2θ of 14.8°, 16.7°, 19.1°, and 22.4°, respectively, for PLA/PBAT/GPOE blends. Two sharp crystalline diffraction peaks located at 2θ=16.7° and 19.1° correlating to the [2, 0, 0/1, 1, 0] and [2, 0, 3] planes, respectively, showed α-form homocrystallite structure of PLA [40,43]. In addition, the reflection pattern [2, 0, 0] showed the typical orthorhombic crystal structure of PLA [40]. The reflections of some weak diffraction peak at 2θ=14.8° [0, 1, 0] and 22.4° [0, 1, 5] also corresponded to the typical α-form of PLA (orthorhombic unit cell) [44]. These results indicate that the presence of GPOE has no impact on the crystalline modification of PLA at the crystallization temperature.

6. Dynamic Mechanical Analysis

Dynamic mechanical analysis was performed to investigate the thermal transitions of the PLA/PBAT/GPOE blends. Fig. 9 shows the tanδ of the PLA/PBAT/GPOE blends from −85 °C to 130 °C. As is known, the temperature corresponding to the peak of tanδ is the glass transition temperature (T_g). As shown in Fig. 9, the 73/30/0 PLA/PBAT/GPOE blend exhibited two distinct glass transition temperatures at −26.1 °C and 63.2 °C corresponding to the PBAT-rich and PLA-rich phases, respectively, indicating that PLA and PBAT were thermodynamically immiscible [33]. All the ternary blend compositions with GPOE exhibit three glass transition temperatures corresponding to the GPOE-rich, PBAT-rich and PLA-rich phases, respectively. When the GPOE content increased, the intensity of the tanδ peaks of the PLA/PBAT/GPOE blends in the low temperature at −42.5 °C that originated from GPOE suffered rose. In addition, with the addition of GPOE the intensity of the tanδ peaks of PBAT and PLA suffered rise and fall, respectively, which corresponded to the content variation in compositions [45]. Note that the T_g of PLA and PBAT shifted increasingly toward each other when the GPOE content increased. The lower

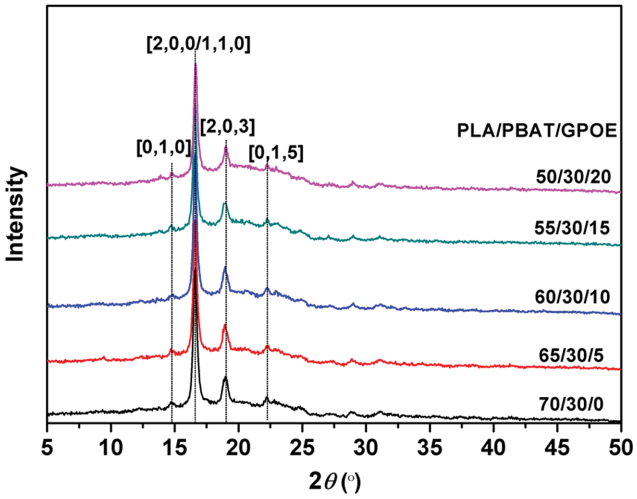

Fig. 8. X-ray diffraction patterns of the PLA/PBAT/GPOE blends.

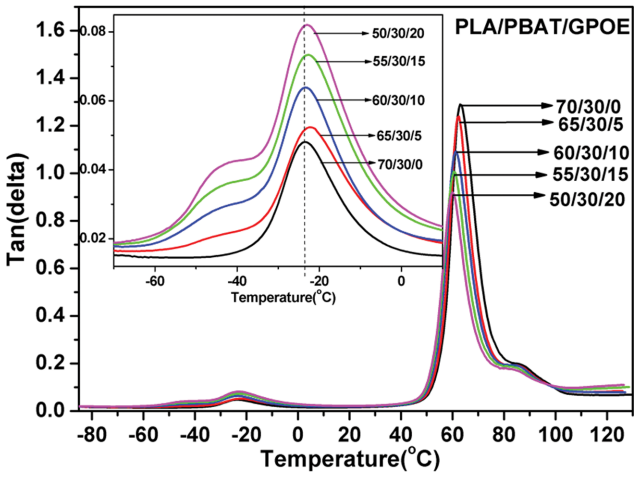

Fig. 9. Plots of the loss factor (tanδ) against the temperature for the PLA/PBAT/GPOE blends.

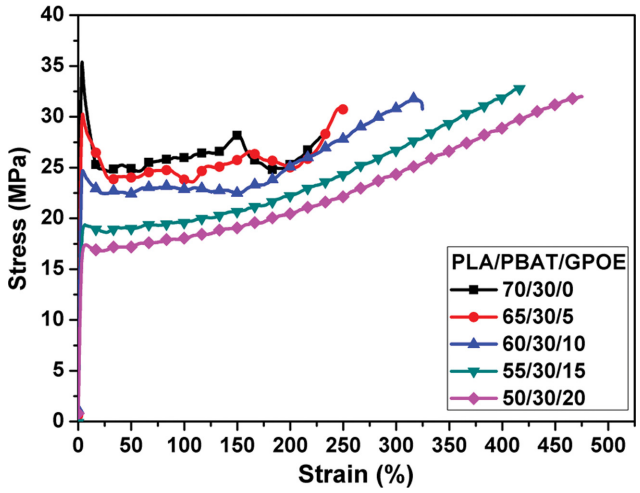

Fig. 10. Tensile behavior of the PLA/PBAT/GPOE blends.

T_g of the PBAT phase in the blends changed from –23.8 °C to –22 °C and the higher T_g of the PLA phase in the blends changed from 63.2 °C to 59.9 °C. The results suggest that GPOE in the blend really modified the miscibility of PLA and PBAT, which resulted from the interfacial interaction between the epoxy group of GPOE with the end group of the PLA and PBAT [46].

7. Mechanical Properties

Typical tensile stress-strain curves of the PLA/PBAT/GPOE blends are shown in Fig. 10 and the mechanical dates are summarized in Table 2. All of the PLA/PBAT/GPOE blends showed clear stress-strain curve yielding behavior and ductile fracture upon tensile load. The addition of GPOE changed the tensile behavior of the blends significantly, as shown in Fig. 10. With increasing GPOE content, stress-strain curve showed more distinct strain hardening, indicating a better delocalization of the strain during tensile testing. The PLA/PBAT/GPOE blend with 70/30/0 w/w/w component presented a tensile strength of 36.2 MPa and an elongation at break of 220%. The incorporation of GPOE resulted in a remarkable increase of elongation at break. When incorporating 5 wt% GPOE into the PLA/PBAT/blend, the corresponding values were 31.9 MPa and 262%. Further addition of GPOE content, i.e., sample 50/30/20 w/w/w PLA/PBAT/GPOE blend showed a two-times higher elongation at break than sample 70/30/0 w/w/w, and the tensile strength had no significant decrease (from 36.2 MPa to 33.1 MPa). These results indicate that GPOE effectively improves the toughness of the polymer blends. The increase in elongation at break and ductility could arise from that the adhesion of interface and the compatibility between PLA and PBAT in the blends were enhanced by the interface interaction with the molecular segments among PLA, PBAT and GPOE.

Young's modulus is another important quantity for evaluating the stiffness of a given material. The addition of GPOE led to a decrease of the modulus value. With increasing GPOE content, the modulus decreased from 1,320 MPa to 650 MPa. It revealed that the addition of the GPOE improved its ductility and softness. In summary, the PLA/PBAT/GPOE blends were less stiff and more ductile than the PLA/PBAT blend regardless of the GPOE content, with this difference becoming progressively more pronounced with increasing GPOE content.

The tensile properties and tear strength of the PLA/PBAT/GPOE films are given in Table 3. The tensile strength of the PLA/PBAT/GPOE film with 70/30/0 w/w/w component was 42.9 MPa in the machine direction (MD) and 36.4 MPa in the transverse direction (TD), and the elongation at break was 114.5% (MD) and 92.6% (TD). With the incorporation of 20 wt% GPOE, a higher elongation yield at break of 256.6% in the MD and 210.4% in the TD was achieved, which was over an increase of 124.1% and 127.2% in comparison to the PLA/PBAT/GPOE film with 70/30/0 w/w/w component. The tensile strength of 50/30/20 w/w/w PLA/PBAT/GPOE film decreased to 32.9 MPa in the MD and 22.5 MPa in the TD, which retained 76.7% and 61.8% of tensile properties of the PLA/PBAT/GPOE film with 70/30/0 w/w/w component, respec-

Table 2. Mechanical properties of the PLA/PBAT/GPOE blends

PLA/PBAT/GPOE (W/W/W)	Tensile strength (MPa)	Elongation at break (%)	Young's modulus (MPa)
70/30/0	36.2±1.1	220±18	1,320±32
65/30/5	31.9±0.5	262±22	1,152±23
60/30/10	32.8±0.9	334±15	949±41
55/30/15	33.8±2.1	425±11	744±18
50/30/20	33.1±1.5	477±27	650±25

Table 3. Mechanical properties of the PLA/PBAT/GPOE films

PLA/PBAT/GPOE (W/W/W)	Tensile strength MD/TD (MPa)	Elongation at break MD/TD (%)	Young's modulus MD/TD (MPa)	Tear strength MD/TD (KN/m)
70/30/0	42.9±6.3/36.4±4.2	114.5±18.2/92.6±15.2	1,347±105/1,217±97	120.1±20.3/135.4±30.1
65/30/5	33.1±3.4/32.4±5.3	147.6±9.7/118.3±19.3	1,089±120/927±74	146.4±8.5/142.8±25.7
60/30/10	35.8±1.7/28.4±0.9	181.5±26.4/146.4±13.2	895±79/837±56	156.5±13.7/178.8±18.9
55/30/15	33.6±4.7/26.5±2.8	215.5±35.1/179.7±23.1	792±43/648±66	148.3±32.4/187.7±18.7
50/30/20	32.9±3.9/22.5±2.2	256.6±12.9/210.4±28.6	676±83/575±73	141.9±23.1/150.3±16.2

tively. The tensile modulus of films in the MD and TD showed a decrement with increasing the GPOE content. The addition of GPOE could improve the tear strength compared with the PLA/PBAT/GPOE film with 70/30/0 w/w/w component. Note that the difference in the values of mechanical properties in the MD and TD could arise from the varying degrees of orientation of the lamellae within the plane of the film [47].

8. Morphology of Fracture Surface

The mechanical property of the blends is closely related to the compatibility between the components, the concentration of the components, and the change in the phase morphology [48]. Fig. 11 shows the cryofracture surfaces of the PLA/PBAT/GPOE blends with various GPOE loadings. Fig. 11(a) shows an SEM image of the PLA/PBAT/GPOE film with 70/30/0 w/w/w component, and a distinct disperse type morphology was seen for the blend. Spherical particles of PBAT were dispersed separately into the continuous PLA matrix, which afforded a typical "sea-island" microstructure, in agreement with the results of Wang et al. [49]. Some gaps were observed between the PBAT and the PLA matrix and the phase interface was very obvious, which was due to the poor miscibility between the two phases [50]. After the addition of 5 wt% content of GPOE, the size of the dispersed PBAT particle become inhomogeneous and some PBAT particles increased obviously; however, the interface between PLA and PBAT become coarse and there are knobs on the surface of PBAT phase. These knobs are the GPOE rich portion of the blends, probably the PLA-co-GPOE-co-PBAT structures located at the PLA-PBAT interphase [51]. As illustrated in Figs. 11(c)-(e), with the addition of GPOE content increasing, the interface between PLA and PBAT became indistinct, as more PLA and PBAT were combined together. The indistinct interface was related to the reduction of the surface tension and improved interfacial adhesion between PLA and PBAT phases. It was concluded that the addition of GPOE improved the interfacial compatibility between PLA and PBAT in the blend. This can be attributed to the interaction of epoxy groups of GPOE with both PLA and PBAT to form PLA-co-GPOE-co-PBAT structures that may play the role of compatibilizer, which is consistent with all the results of the above sections.

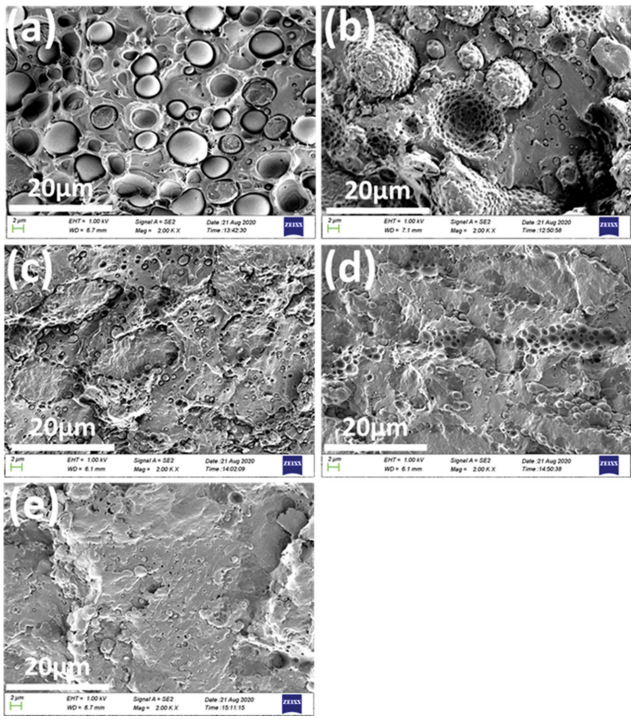

Fig. 11. SEM images of the fractured surface morphology (immersion in liquid nitrogen) of the PLA/PBAT/GPOE blends with different GPOE content: (a) 0 wt%, (b) 5 wt%, (c) 10 wt%, (d) 15 wt% and (e) 20 wt%.

9. Thermal Stability

An estimation of the thermal resistance of the PLA/PBAT/GPOE films was made by TGA/DTG. Fig. 12 shows the TGA and DTG curves for the PLA/PBAT/GPOE films with different content of GPOE. Table 4 summarizes the 10% weight-loss temperature ($T_{10\%}$) and the 50% weight-loss temperature ($T_{50\%}$) of the PLA/PBAT/GPOE films. According to the TGA/DTG analysis, we noticed two degradation processes for the PLA/PBAT/GPOE film without GPOE. When GPOE was added in PLA/PBAT blends, three degradation processes for the PLA/PBAT/GPOE films with 5-20 wt% GPOE were observed. By comparing those degradation processes with neat PLA, PBAT and GPOE, we can conclude that the first peak is the decomposition of the degradation of PLA-rich

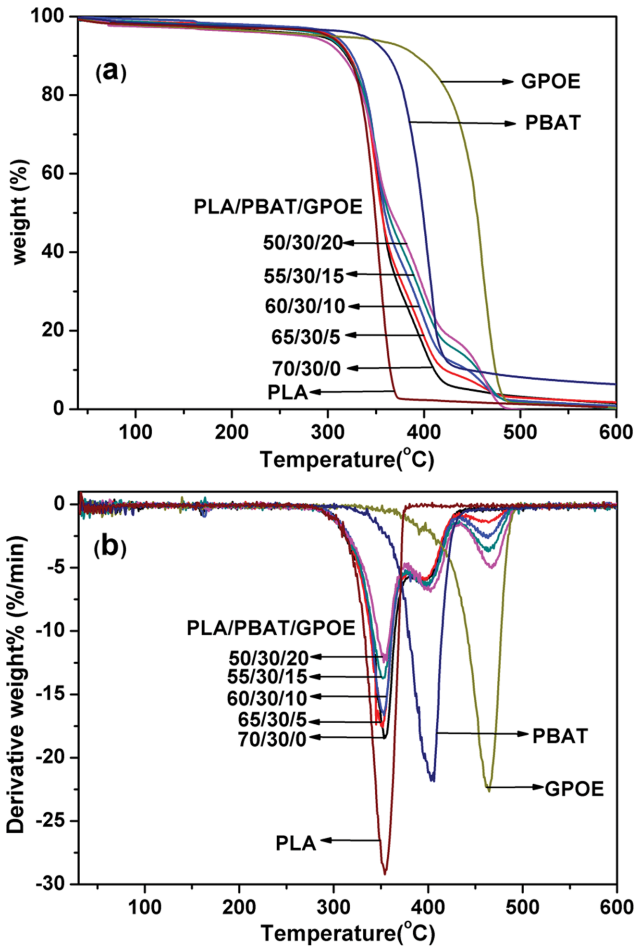

Fig. 12. (a) TGA curves and (b) DTG curves of the PLA/PBAT/GPOE films under nitrogen.

Table 4. Result of thermogravimetric analysis of the PLA/PBAT/GPOE films

PLA/PBAT/GPOE (w/w/w)	$T_{10\%}$ (°C)[a]	$T_{50\%}$ (°C)[b]	T_{max} (°C)[c]		
			Step 1	Step 2	Step 3
PLA	321.2	349.1	354.1	-	-
PBAT	363.1	398.9	-	404.6	-
GPOE	392.0	454.2	-	-	464.5
70/30/0	319.1	355.2	354.4	396.2	-
65/30/5	322.5	356.1	351.1	399.1	463.4
60/30/10	325.3	359.6	353.6	398.9	464.4
55/30/15	320.8	362.6	351.9	399.7	465.2
50/30/20	318.6	369.5	354.4	402.3	466.8

[a]Temperature at 10% mass loss
[b]Temperature at 50% mass loss
[c]Temperature at maximum degradation rate

phase. The second peak is related to the degradation of PBAT-rich phase and, finally, the third peak is associated with GPOE thermal degradation. As shown in Table 4, $T_{10\%}$ of the PLA/PBAT/GPOE films containing different content of GPOE had no obvious change; however, $T_{50\%}$ of the PLA/PBAT/GPOE films increased with increasing GPOE content. Therefore, the effect of GPOE on the thermal stability of the blend films was that GPOE enhanced thermal stability of the PLA/PBAT/GPOE films, which was attributed to the effective chemical reaction between PBAT and PLA promoted by GPOE.

10. Water Vapor Permeability of Films

Table 5 shows the water vapor permeability (WVP) of blend films. For the pure PLA and PBAT, the WVP values were 9.13×10^{-14} and 27.8×10^{-14} g·cm/cm^2·Pa·s, while the WVP value of GPOE was 1.64×10^{-14} g·cm/cm^2·Pa·s. The WVP values of PLA and PBAT were higher than that of GPOE, which shows that PLA and PBAT have better water vapor permeability than GPOE. This difference may be ascribed to specific interactions (hydrogen bonds) between incoming water molecules and polar groups (ester functions) in chain backbone of PLA and PBAT, increasing the water affinity of the film [52,53], and the better water affinity improved water vapor permeability. For blend films, WVP values showed a noticeable reduction when GPOE content increased from 0 to 20 wt%. Except that the addition of GPOE with low WVP value caused the WVP values of blend films to decrease; another factor contributing to the decrease in WVP values of blend films was that addition of GPOE improved the interfacial compatibility of blend, which could decrease channel of water molecular in blend. This result indicated that GPOE could effectively improve the water vapor barrier property of blend films.

Table 5. The WVP values of the PLA/PBAT/GPOE films

PLA/PBAT/GPOE (w/w/w)	WVP ($\times10^{-14}$ g·cm/cm^2·Pa·s)
PLA	9.13
PBAT	27.8
GPOE	1.64
70/30/0	12.9
65/30/5	10.3
60/30/10	9.79
55/30/15	6.75
50/30/20	5.93

CONCLUSIONS

GPOE incorporated PLA and PBAT based blends and films were fabricated successfully. GPOE as the reactive compatibilizer can enhance the compatibility between PLA and PBAT. Rheological and melt strength results showed that the addition of GPOE increased storage modulus (G′), loss modulus (G″), complex viscosity (η^*) and melt strength. From DSC and DMA results we can know that PLA and PBAT blend is a thermodynamically immiscible system; however, the addition of GPOE can improve the compatibility. WAXD analyses revealed that crystalline modification of PLA at the crystallization temperature had not changed significantly. However, POM observations showed that the addition of GPOE increased the density of spherulite nucleation and afforded smaller spherulites. The mechanical properties of blends and films were enhanced by the addition of GPOE. The elongation at break of blends and films was improved more than twice after addition of 20 wt% GPOE compared to system without GPOE, and the tensile strength had no significant decrease. Moreover, the interaction and compatibility at the interface between PLA and PBAT were improved by the addition of compatibilizer GPOE, as shown in the SEM result. Moreover, the addition of GPOE also can enhance thermal stability of blend films and improve the water vapor barrier property of blend films. In conclusion, GPOE was determined to be an ideal compatibilizer for PLA/PBAT blends.

ACKNOWLEDGEMENTS

This work was financially supported by the fund of Science and Technology Bureau of Jilin Province of China (No. 20170204012SF), Chinese Academy of Sciences (Changchun Branch) (No. 2020SYHZ0002 and No. 2020SYHZ0047), Science and Technology Services Network Program of Chinese Academy of Sciences (STS

Project) (No. KFJ-STS-ZDTP-082), and the National Science Foundation of Zhejiang Province of China (No. LQY19B040001).

REFERENCES

1. B. Palai, S. Mohanty and S. K. Nayak, *Polym. Test.*, **83**, 106130 (2020).
2. M. Nofar, R. Salehiyan, U. Ciftci, A. Jalali and A. Durmus, *Compos. Part B-Eng.*, **182**, 107661 (2020).
3. Y. Zhou, J. Wang, S.-Y. Cai, Z.-G. Wang, N.-W. Zhang and J. Ren, *Polym. Bull.*, **75**, 5437 (2018).
4. R. G. F. Costa, G. S. Brichi, C. Ribeiro and L. H. C. Mattoso, *Polym. Bull.*, **73**, 2973 (2016).
5. P. Agrawal, A. P. M. Araújo, J. C. C. Lima, S. N. Cavalcanti, D. M. G. Freitas, G. M. G. Farias, M. M. Ueki and T. J. A. Mélo, *J. Polym. Environ.*, **27**, 1439 (2019).
6. S. Pilla, S. G. Kim, G. K. Auer, S. Gong and C. B. Park, *Polym. Eng. Sci.*, **49**, 1653 (2009).
7. L.-Q. Xu and H.-X. Huang, *Ind. Eng. Chem. Res.*, **53**, 2277 (2014).
8. S. Wang, S. Pang, L. Pan, N. Xu and T. Li, *Polymers*, **8**, 417 (2016).
9. S. Phattarateera and C. Pattamaprom, *J. Polym. Environ.*, **28**, 1592 (2020).
10. Z. Wang, M. Zhang, Z. Liu, S. Zhang, Z. Cao, W. Yang and M. Yang, *J. Appl. Polym. Sci.*, **135**, 46009 (2018).
11. J.-Z. Li, J. M. Schultz and C. M. Chan, *Polymer*, **63**, 179 (2015).
12. Y. Eom, B. Choi and S.-i. Park, *J. Polym. Environ.*, **27**, 256 (2018).
13. H. Fang, F. Jiang, Q. Wu, Y. Ding and Z. Wang, *ACS Appl. Mater. Inter.*, **6**, 13552 (2014).
14. R. Li, L. Wu and B.-G. Li, *Ind. Eng. Chem. Res.*, **56**, 2773 (2017).
15. T. R. Rigolin, L. C. Costa, M. A. Chinelatto, P. A. R. Muñoz and S. H. P. Bettini, *Polym. Test.*, **63**, 542 (2017).
16. R. Al-Itry, K. Lamnawar and A. Maazouz, *Polym. Degrad. Stabil.*, **97**, 1898 (2012).
17. F.-L. Jin, R.-R. Hu and S.-J. Park, *Korean J. Chem. Eng.*, **37**, 905 (2020).
18. N. Chuaponpat, T. Ueda, A. Ishigami, T. Kurose and H. Ito, *Polymers*, **12**, 1083 (2020).
19. M. Zhang and N. L. Thomas, *Adv. Polym. Tech.*, **30**, 67 (2011).
20. T. Takayama and M. Todo, *J. Mater. Sci.*, **41**, 4989 (2006).
21. X. Ma, J. Yu and N. Wang, *J. Polym. Sci. Pol. Phys.*, **44**, 94 (2006).
22. W. Song, H. Liu, F. Chen and J. Zhang, *Polymer*, **53**, 2476 (2012).
23. C. M. Lee, E. S. Kim and J.-S. Yoon, *J. Appl. Polym. Sci.*, **98**, 886 (2005).
24. M. Nofar, M. Mohammadi and P. J. Carreau, *J. Appl. Polym. Sci.*, **137**, e49387 (2020).
25. Y. Deng, C. Yu, P. Wongwiwattana and N. L. Thomas, *J. Polym. Environ.*, **26**, 3802 (2018).
26. L. Jiang, M. Wolcott and J. Zhang, *Biomacromolecules*, **7**, 199 (2006).
27. G. Ting, D. Zhu, Y. Lu and S. Lu, *Polym. Sci. Ser. A*, **61**, 317 (2019).
28. N. Zhang, C. Zeng, L. Wang and J. Ren, *J. Polym. Environ.*, **21**, 286 (2012).
29. H. He, G. Wang, M. Chen, C. Xiong, Y. Li and Y. Tong, *Materials*, **13**, 2094 (2020).
30. X. Wang, S. Peng, H. Chen, X. Yu and X. Zhao, *Compos. Part B-Eng.*, **173**, 107028 (2019).
31. L. T. Lim, R. Auras and M. Rubino, *Prog. Polym. Sci.*, **33**, 820 (2008).
32. J. Andrzejewski, J. Cheng, A. Anstey, A. K. Mohanty and M. Misra, *ACS Sustain. Chem. Eng.*, **8**, 6576 (2020).
33. Y. Ding, B. Lu, P. Wang, G. Wang and J. Ji, *Polym. Degrad. Stabil.*, **147**, 41 (2018).
34. Z. Sun, B. Zhang, X. Bian, L. Feng, H. Zhang, R. Duan, J. Sun, X. Pang, W. Chen and X. Chen, *RSC Adv.*, **5**, 73842 (2015).
35. X. Li, X. Ai, H. Pan, J. Yang, G. Gao, H. Zhang, H. Yang and L. Dong, *Polym. Adv. Technol.*, **29**, 1706 (2018).
36. Z. Su, Q. Li, Y. Liu, G.-H. Hu and C. Wu, *Eur. Polym. J.*, **45**, 2428 (2009).
37. L. C. Arruda, M. Magaton, R. E. S. Bretas and M. M. Ueki, *Polym. Test.*, **43**, 27 (2015).
38. X. Wang, J. Mi, J. Wang, H. Zhou and X. Wang, *RSC Adv.*, **8**, 34418 (2018).
39. L. Aliotta, V. Gigante, O. Acucella, F. Signori and A. Lazzeri, *Front. Mater.*, **7**, 130 (2020).
40. A. K. Pal and V. Katiyar, *Biomacromolecules*, **17**, 2603 (2016).
41. J. Bai, J. Wang, W. Wang, H. Fang, Z. Xu, X. Chen and Z. Wang, *ACS Sustain. Chem. Eng.*, **4**, 273 (2015).
42. F. Qi, M. Tang, X. Chen, M. Chen, G. Guo and Z. Zhang, *Eur. Polym. J.*, **71**, 314 (2015).
43. H. Wang, J. Yu, H. Fang, H. Wei, X. Wang and Y. Ding, *Polymer*, **137**, 1 (2018).
44. H. Zhang, S. Wang, S. Zhang, R. Ma, Y. Wang, W. Cao, C. Liu and C. Shen, *Polym. Test.*, **64**, 12 (2017).
45. W. Lin and J.-P. Qu, *Ind. Eng. Chem. Res.*, **58**, 10894 (2019).
46. A.-L. Hou and J.-P. Qu, *Polymers*, **11**, 771 (2019).
47. Y. Zhao, X. Lang, H. Pan, Y. Wang, H. Yang, H. Zhang, H. Zhang and L. Dong, *Polym. Eng. Sci.*, **55**, 2801 (2015).
48. X. Yu, X. Wang, Z. Zhang, S. Peng, H. Chen and X. Zhao, *Polym. Test.*, **78**, 105980 (2019).
49. B. Wang, Y. Jin, K. e. Kang, N. Yang, Y. Weng, Z. Huang and S. Men, *e-Polymers*, **20**, 39 (2020).
50. D. Wu, Y. Guo, A. Huang, R. Xu and P. Liu, *Polym. Bull.* (2020).
51. N. T. Kilic, B. N. Can, M. Kodal and G. Ozkoc, *Appl. Polym. Sci.*, **136**, 47217 (2019).
52. M. Ilsouk, M. Raihane, B. Rhouta, R. M. Meri, J. Zicans, J. Vecstaudza and M. Lahcini, *RSC Adv.*, **10**, 37314 (2020).
53. N. Follain, R. Cretois, L. Lebrun and S. Marais, *Phys. Chem. Chem. Phys.*, **18**, 20345 (2016).